*Polymers* **2014**, *6*, 300-310; doi:10.3390/polym6020300

OPEN ACCESS

*polymers*

**ISSN 2073-4360**

www.mdpi.com/journal/polymers

*Article*

# Enhancement Corrosion Resistance of (γ-Glycidyloxypropyl)-Silsesquioxane-Titanium Dioxide Films and Its Validation by Gas Molecule Diffusion Coefficients Using Molecular Dynamics (MD) Simulation

**Haiyan Wang [1], Li Liu [1], Yudong Huang [1], Di Wang [2], Lijiang Hu [1,*] and Douglas A. Loy [3]**

[1] School of Science; School of Chemical Engineering; Harbin Institute of Technology, Harbin 150001, China; E-Mails: wangsy2009@126.com (H.W.); liuli@hit.edu.cn (L.L.); huangyd@hit.edu.cn (Y.H.)

[2] Material Science and Engineering College, Northeast Forestry University, Harbin 150040, China; E-Mail: diwang1030@126.com

[3] Department of Materials Science and Engineering, The University of Arizona, Tucson, AZ 85721, USA; E-Mail: daloy@mse.arizona.edu

* Author to whom correspondence should be addressed; E-Mail: hulijiang2008@126.com; Tel.: +86-451-8641-2679; Fax: +86-451-8622-1048.

*Received: 28 November 2013; in revised form: 17 January 2014 / Accepted: 20 January 2014 / Published: 27 January 2014*

---

**Abstract:** Based on silsesquioxanes (SSO) derived from the hydrolytic condensation of (γ-glycidyloxypropyl)trimethoxysilane (GPMS) and titanium tetrabutoxide (TTB), hybrid films on aluminum alloy (AA), film-GPMS-SSO (f-GS) and f-GS-$TTB_{i\%}$ (f-$GSTT_{5\%–25\%}$, $i$ = 5, 10, 15, 20 and 25 wt%), were prepared and tested by electrochemical measurements with typical potentiodynamic polarization curves. The $I_{corr}$ values of the samples were significantly lower, comparing with the $I_{corr}$ values of the f-GS, AA and f-GS modified tetraethoxysilane (TEOS) in the previous study, which implies that the $TTB_{5\%–25\%}$ ($TiO_2$) additions in the coatings indeed enhance the electrochemical corrosion resistance. Correlations between the film structures and anticorrosion properties were discussed. To validate the corresponding anticorrosion experiment results, different 3D-amorphous cubic unit cells were employed as models to investigate the self-diffusion coefficient (SDC) for $SO_2$, $NO_2$ and $H_2O$ molecules by molecular dynamics (MD) simulation. All of the SDCs calculated for $SO_2$, $NO_2$ and $H_2O$ diffusing in f-$GSTT_{5\%–25\%}$ cells were less than the SDCs in f-GS. These results validated the corresponding anticorrosion experiment results.

**Keywords:** silsesquioxane film; titanium; anticorrosion; molecule dynamics simulation

## 1. Introduction

Silsesquioxane (SSO) compounds have an important role in applications requiring thin film [1–3]. Due to their nanostructure and superior properties, these attractive engineering materials provide new strategies to incorporate and release corrosion inhibitors, allowing toxic and hazardous hexavalent chromium-containing compounds to be replaced [4].

However, SSO films have a higher probability of being porous, compliant and incompletely crosslinked, formed in the courses of hydrolytic condensation and final curing [5,6]. These structural characteristics can facilitate transport of small gas molecules into the film surface where corrosion occurs and limits the efficacy of the hybrid films. In the previous study [7,8], silsesquioxanes (SSO) derived from hydrolytic condensation of (γ-glycidyloxypropyl)trimethoxysilane (GPMS) and (γ-methacryloxylpropyl)trimethoxysilane (MPMS) modified with tetraethoxysilane (TEOS) were investigated as anticorrosion coatings on bare aluminum alloys (AA). TEOS was added into the reaction systems to enhance the density of the films, and expected anticorrosion properties were obtained from the TEOS (or $SiO_2$ after the hydrolytic condensation of TEOS) modified systems.

Titanium-hybrids with organic epoxide resins have been used as protective coatings to take advantage of their superior mechanical properties and adhesion to metals [9,10]. Hybrids based on (γ-glycidyloxypropyl)silsesquioxanes (GS) and modified with titanium tetrabutoxide **(**TTB, or $TiO_2$ after the hydrolytic condensation of TTB) have been prepared [11,12], but generally include additional metal oxides and silica. In this work, GS films are investigated as anticorrosion coatings on AA, and just TTB is added into the reaction system to enhance the density and corrosion resistance of f-GS. One focus of this work is the correlation between the film structure and the anticorrosion properties of the modified films which act as corrosion inhibitors and enhance the corrosion resistance.

In addition to the synthesis and anticorrosion experimental component, this study is to validate the corresponding anticorrosion-experiment results, using a sample model of molecular dynamics (MD) simulations which have recently been successfully used to estimate the self-diffusion coefficients of small gas molecules in models of hybrid materials [13,14]. To demonstrate the MD simulation accurately enough to predict the self-diffusion coefficient of small gas molecules in amorphous hybrid materials, the calculation, minimization and equilibration of the simulated structure should be performed during the MD simulation method [15,16]. For the validation, a hybrid microstructure similar to the polymer microstructure reported in the literature is employed to investigate self-diffusion coefficients by MD simulation for $NO_2$, $SO_2$ and $H_2O$ molecules [15,16].

## 2. Experimental Section

### *2.1. Materials*

Commercial GPMS (Dow Corning Z-60406040, Beijing, China) was used in the study of hydrolytic condensation reactions; TTB (97.0%) employed as a modifier, formic acid (HCOOH, 98%) used as a

catalyst, ethanol ($C_2H_5OH$, 99.7%) used as a solvent and ethylenediamine (EDA, 98%) selected as the hardener were analytical grade reagents, obtained from the Tianjin Chemicals, China.

### *2.2. Preparation of Films*

To prepare the sols, GPMS and TTB were pre-hydrolyzed separately. GPMS was hydrolyzed in ethanol with formic acid (0.5:1, formic acid:GPMS) for 5 days at 40 °C. The resulting GPMS-SSO will be denoted as GS. TTB was hydrolyzed in ethanol with hydrochloric acid (0.05:1, HCl:TTB) for 4 days at 40 °C. The mole ratios of ethanol and $H_2O$ with respect to both Si and Ti were 4 and 3, respectively. Next, the hydrolyzed GPMS and TTB (5, 10, 15, 20 and 25 wt%) sols were combined and stirred continuously for 5 h at 35 °C. The GS modified with TTBs will be denoted as $GSTT_{i\%}$ or $GSTT_{5\%–25\%}$.

The resulting GS and $GSTT_{5\%–25\%}$ was diluted with ethanol (molar ratio $Si/C_2H_5OH$ = 1/4) and then a theoretical amount of EDA was added. Dip-coating on the AA (40 × 10 × 2 mm) was performed three times at 6-hour intervals with a dipping speed of 300 mm/min. After dipping, the coated samples were put into a heating oven for 6 h at 80 °C followed by 4 h at 120 °C. The hard and transparent films coated on AA will be denoted as f-GS and f-$GSTT_{5\%–25\%}$.

### *2.3. Electrochemical Measurements [8]*

Electrochemical measurements were performed using a CHI 630 device and a three-electrode cell equipped with a saturated calomel reference electrode (SCE), a platinum counter electrode and a coated or non-coated AA panel as the working electrode having an exposed area of 1.0 $cm^2$. All measurements were conducted in an aqueous 3.5 wt% NaCl working solution at room temperature. The electrodes were kept in the working solution for 30 min prior to measurements with the electrical circuit opened. 352 SoftCorr III corrosion measurement software (EG&G Princeton Applied Research, Princeton, NJ, USA) was used to analyze the potentiodynamic polarization curves. A potential scanning range was −1–1.2 V with a scanning rate of 2 mv/s.

The surface morphology of the corroded films and the film thickness (2 μm) were examined with scanning electron microscopy (SEM, Hitachi S-4700, Tianmei, Beijing, China).

## 3. Computational Methodology

The models were generated with Amorphous Cell program of Material Studio software (MSS) of Accelrys Inc. (San Diego, CA, USA) The films, sandwiched between superstrate (air) and a substrate (aluminium alloy), were modeled in a cell together with small gas molecules. The generated network models consisted of 5 different 3D-amorphous cubic unit cells with periodic boundary conditions, containing oligomers based on GS, modifiers ($TiO_2$) and gas molecules ($SO_2$, $NO_2$ and $H_2O$). Cells based on f-$GSTT_{i\%}$ ($i$ = 0, 5, 10, 15, 20 and 25 wt%) [denote cell(f-$GSTT_{0\%–25\%}$)] were constructed with each kind of cell containing three different gas molecules, respectively. As seen in Figure 1a–e, cell(f-$GSTT_{0\%–25\%}$) contained 10 oligomers (GS), 8 $SO_2$s, 8 $NO_2$s and 8 $H_2O$s for each; and contained 8, 16, 24, 32 and 40 $TiO_2$s for the cell(f-$GSTT_{5\%–25\%}$), respectively. The density for every

cell was fixed to about 1.00 g/cm$^3$ based on total molecular weights of molecules in a cell and the auto-adjusted cell volume [8,17,18].

**Figure 1.** Model cells for f-GSTT$_{i\%}$ ($i$ = 0, 5, 10, 15, 20 and 25 wt%) containing GS oligomers, $H_2O$, $NO_2$ and $SO_2$ gas molecules, and 5–25 wt% $TiO_2$ modifiers, respectively.

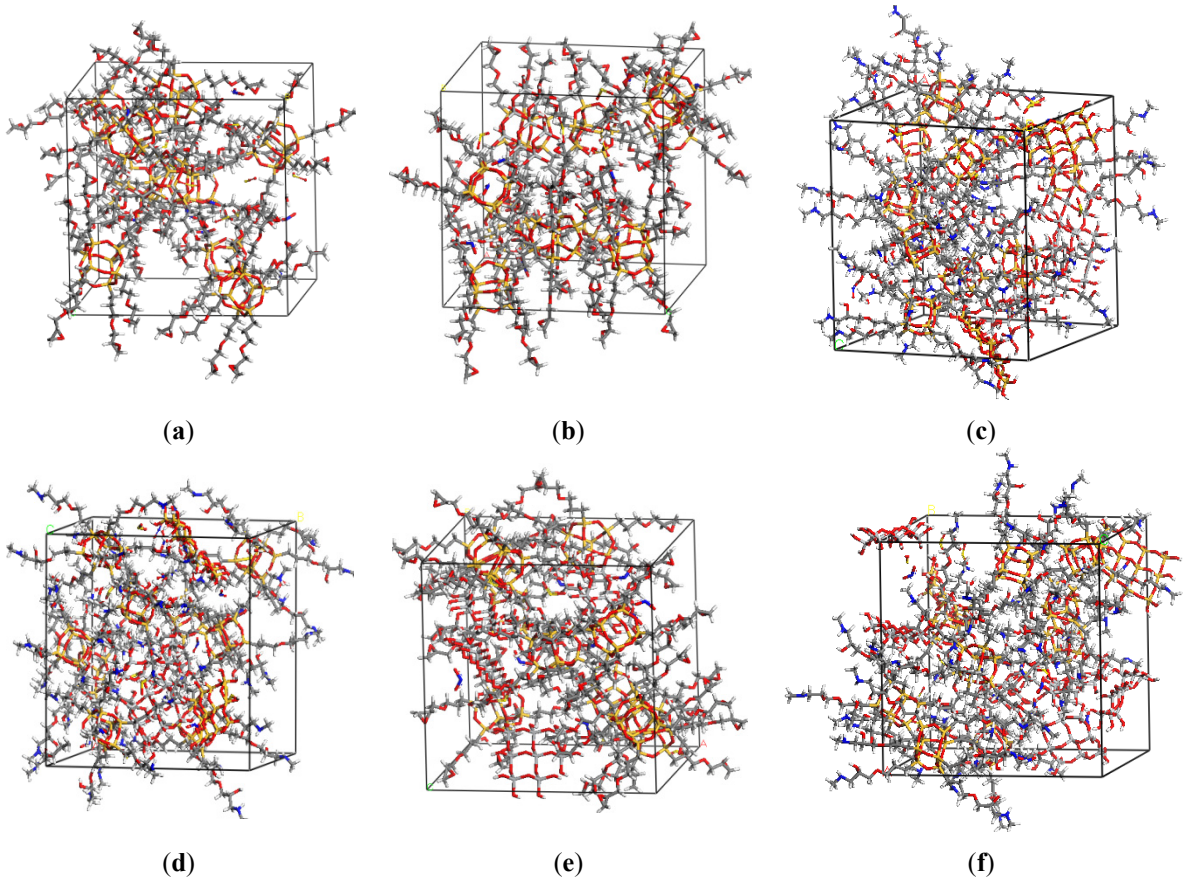


Meunier reported the estimation of SDC of small gas molecules in an amorphous polymer under different reaction and microstructure conditions, employing MD simulations [15]. The SDC were calculated from the mean-square displacement (MSD) of the penetrant molecules by means of the Einstein equation [15,16]:

$$D_\alpha = \frac{1}{6N_\alpha}\lim_{t\to\infty}\frac{d}{dt}\sum_{i=1}^{N_\alpha}\left\langle\left[r_i(t)-r_i(0)\right]^2\right\rangle \quad (1)$$

$$\mathrm{MSD} = \left\langle\left|r(t)-r(0)\right|^2\right\rangle \quad (2)$$

where, $N_\alpha$ is the number of diffusing atoms, $r(0)$ is an initial position vector of the penetrant molecule in the selected hybrid microstructure, $r(t)$ is the position vector of this molecule after time $t$, and $|r(t) - r(0)|$ represents the displacement of the penetrant molecule during time $t$. Equation (1) assumes that the SDC is a constant, *i.e.*, independent of the penetrant gas concentration in the polymer. The MSD, $|r(t) - r(0)|^2$, of $SO_2$, $NO_2$ and $H_2O$ were calculated from the trajectories of the gas molecules $SO_2$, $NO_2$ and $H_2O$ in the hybrid microstructures.

## 4. Results and Discussion

### *4.1. Corrosion Resistance of Modified Hybrid Films*

The anticorrosive performance of films can be examined from the corrosion current density ($I_{corr}$) obtained from the intersection of the anodic and cathodic Tafel curves (potentiodynamic polarization curves) [19–21]. Figure 2 shows the typical potentiodynamic polarization curves of different specimens, f-GSTT$_{i\%}$ ($i$ = 0, 5, 10, 15, 20 and 25), in an aqueous 3.5 wt% NaCl working solution at room temperature. The current densities of f-GSTT$_{5\%–25\%}$ (5%:2.37, 10%:0.82, 15%:0.43, 20%:0.10 and 25%:0.093 nA/cm$^2$, respectively) are significantly different with the orders of f-GSTT$_{25\%}$ < f-GSTT$_{20\%}$ < f-GSTT$_{15\%}$ < f-GSTT$_{10\%}$ < f-GSTT$_{5\%}$ and lower than the densities of f-GSTT$_{0\%}$ or f-GS (0%:1550.00 nA/cm$^2$), bare AA (5755.00 nA/cm$^2$) [4,8] and f-GSTE$_{5\%–30\%}$ [4,7]. At the same weight percent loading of titanium dioxide as silica in the f-GSTE$_{10\%}$ sample, the f-GSTT$_{10\%}$ sample exhibited a corrosion current density that was 200 times smaller [19], which implies that the titanium dioxide modified films indeed provide a greater improved barrier for blocking the electrochemical corrosion process.

**Figure 2.** Typical polarization curves of film-GPMS-SSO (f-GS) (aa') f-GSTT$_{5\%}$ (bb'), f-GSTT$_{10\%}$ (cc'), f-GSTT$_{15\%}$ (dd'), f-GSTT$_{20\%}$ (ee') and f-GSTT$_{25\%}$ (ff'). The data were measured in 3.5 wt% NaCl aqueous solution.

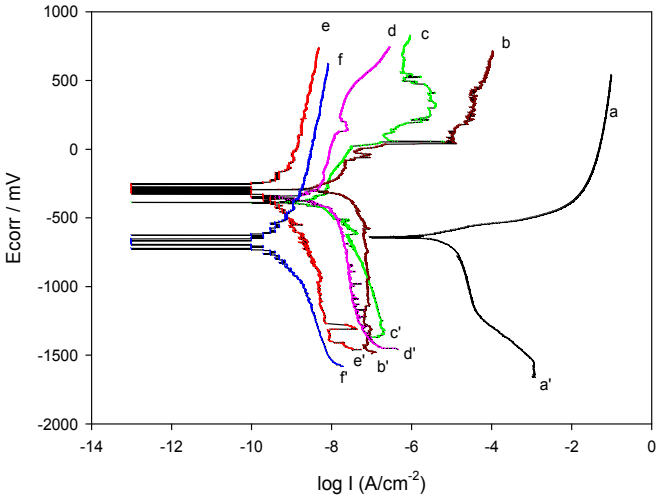


### *4.2. Correlation between the Film Structure and Anticorrosion Properties*

The SSO film structures and processing conditions strongly influence the anticorrosion properties of coatings. A f-GSTT network based on organic/inorganic hybrids undergoing extensive cross-linking would lead to the formation of a dense coating with enhanced anticorrosion properties relative to AA, f-GS or f-GSTT. The protection efficiency ($P$) of the sol-gel coatings on AA could be similarly calculated by the equation [22]:

$$P\ (\%) = 100\ (1 - I_{corr}/I_{AA}) \quad (3)$$

where $I_{AA}$ and $I_{corr}$ denote the corrosion current density of the bare AA and coated AA, respectively.

In Figure 2, the f-GSTT$_{5\%}$ and f-GSTT$_{10\%}$ current–voltage curves show a distinct active-passive transition; the absence of the passivation region in the f-GSTT$_{20\%}$ and f-GSTT$_{25\%}$ curves indicates that

the anticorrosion properties of f-GSTT mainly result from the barrier provided by the addition of TTB, which prevents the oxidation on the AA surface [23,24]. An adequate amount of TTB modifier can support f-GS to fabricate a denser structure that significantly improves the anticorrosion properties of coatings. This enhanced anticorrosion effect of f-GSTT might have arisen from dispersing $TiO_2$ dense particles and organic fractions in an f-GSTT matrix to block the diffusion pathway of corrosive penetrants. In a sense, the penetrate molecules have a longer more tortuous path when inorganic particles are present. These barrier effects have been thoroughly documented with permeability of gas molecules $O_2$ and $H_2O$ through PMMA-clay nanocomposite membranes [25]. The origin of the protection offered by the hybrid coatings is clearly due to their barrier properties. Noise in f-GSTT current-voltage curves results from the formation of pits in the AA surface coating of a very thin organic film.

As was predicted by the SEM analysis in Figure 3 and recapitulated by the above electrochemical analyses, the electron micrographs of f-GS (Figure 3a) show the open cell, micron-scale porosity that would permit water and salts access to the underlying metal, providing the least protection to the aluminum substrate. Corrosion of aluminum protected by the f-$GSTT_{5\%–25\%}$ is less prevalent, because the $TiO_2$ modifiers in f-$GSTT_{5\%–25\%}$ result in a denser structure that significantly improves the anticorrosion properties of coatings. Obvious corrosion and delamination phenomena were observed in the f-$GSTT_{5\%–15\%}$ surfaces (Figure 3b–d), but are almost absent in the f-$GSTT_{20\%}$ and f-$GSTT_{25\%}$ surfaces with few cracks (Figure 3e,f), due to the greater volume of the $TiO_2$ modifiers that ultimately result in denser, less permeable coatings. For perspective, the SEM image of Figure 1f shows that 25% TTB results in a very smooth coating, which enhance anticorrosion properties of the f-GS and renders f-$GSTT_{25\%}$ suitable for and more effective as protective coatings.

**Figure 3.** Scanning electron microscopy (SEM) images (20 kV, 9800, 38 lm, ×200) of six samples for electrochemistry measurements: (**a**) f-GS; (**b**) f-$GSTT_{5\%}$; (**c**) f-$GSTT_{10\%}$; (**d**) f-$GSTT_{15\%}$; (**e**) f-$GSTT_{20\%}$ and (**f**) f-$GSTT_{25\%}$.

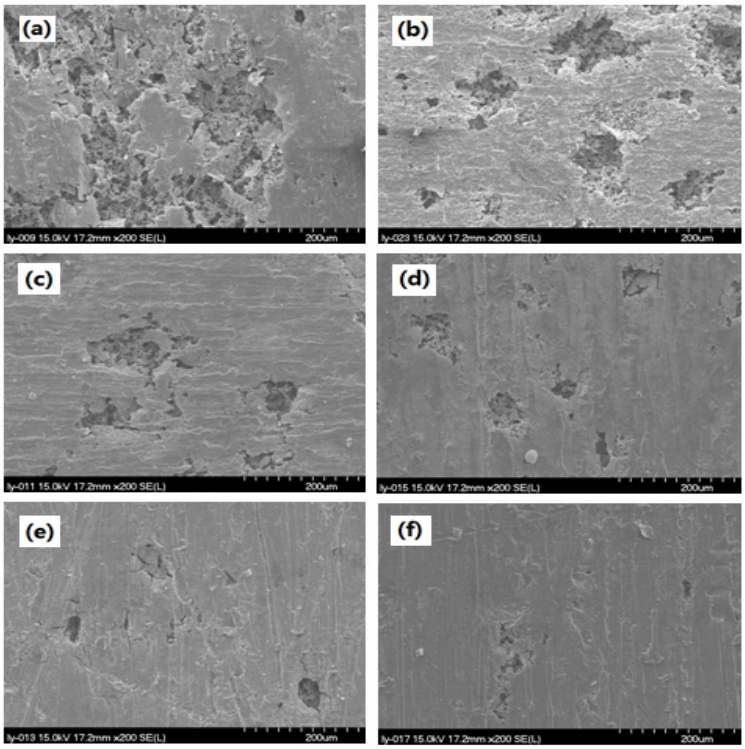

### *4.3. Verification of Enhancement Corrosion Resistance by SDC Using MD Simulation*

In addition to the experimental assessment of the protective characteristics of the f-GSTT, it was possible to use computer modeling to simulate the performance of the films and validate the model for beneficial effects of the titanium dioxide. For corrosion to occur on the aluminum surface, there needs to be water and some Lewis acid, such as sulfur dioxide or nitrogen dioxide. The more a coating permits these molecules to permeate to the metal surface, the greater the corrosion will be. So the simulations involve constructing a model piece of the coating structure and measuring the diffusion of $SO_2$, $NO_2$ and $H_2O$ molecules. Table 1 lists the values of the SDC for the $SO_2$, $NO_2$ and $H_2O$ molecules in cell(f-GSTT$_{0\%–25\%}$) at room temperature, calculated with Equations (1) and (2). The SDC values in cell(f-GSTT$_{5\%–25\%}$) are much less than the values in cell(f-GS/TEOS) [18], indicating a more compact structure. Figure 4a–c show plots of MSD of $SO_2$, $NO_2$ and $H_2O$ molecules in cell(f-GSTT$_{0\%–25\%}$) as a function of time, obtained from MD simulations. According to Equation (1), a plot of MSD *versus* time should be linear if SDC is constant. All estimated SDCs were determined from the slopes of the plots. Figure 4a shows curves for $H_2O$ of which the slopes are bigger than those of the curves for $SO_2$ and $NO_2$. This result can be ascribed to the lower molecular weight and size of $H_2O$ compared with $SO_2$ and $NO_2$, leading to bigger SDCs of $H_2O$ in cell(f-GSTT$_{0\%–25\%}$). More $H_2O$ molecules can diffuse onto the AA surface ahead of the diffusion of $SO_2$ and $NO_2$ and the excess $H_2O$ molecules combine with the $SO_2$ and $NO_2$ on the AA surface to form corrosive species.

**Table 1.** Estimated self-diffusion coefficient (SDC) for $SO_2$, $NO_2$ and $H_2O$ in cell(f-GSTT$_{0\text{-}25\%}$) respectively.

| Cells | Penetrant | Slope | SDC ($10^{-8}$·cm$^2$·s$^{-1}$) |
|---|---|---|---|
| f-GS | $H_2O$ | 5.27 | 0.88 |
| | $NO_2$ | 3.99 | 0.66 |
| | $SO_2$ | 2.81 | 0.47 |
| f-GSTT$_{5\%}$ | $H_2O$ | 4.26 | 0.71 |
| | $NO_2$ | 2.93 | 0.49 |
| | $SO_2$ | 2.04 | 0.34 |
| f-GSTT$_{10\%}$ | $H_2O$ | 3.76 | 0.63 |
| | $NO_2$ | 2.52 | 0.42 |
| | $SO_2$ | 1.76 | 0.29 |
| f-GSTT$_{15\%}$ | $H_2O$ | 3.23 | 0.54 |
| | $NO_2$ | 2.18 | 0.36 |
| | $SO_2$ | 1.53 | 0.26 |
| f-GSTT$_{20\%}$ | $H_2O$ | 2.66 | 0.44 |
| | $NO_2$ | 1.81 | 0.30 |
| | $SO_2$ | 1.26 | 0.21 |
| f-GSTT$_{25\%}$ | $H_2O$ | 2.05 | 0.34 |
| | $NO_2$ | 1.37 | 0.23 |
| | $SO_2$ | 1.06 | 0.18 |

**Figure 4.** Mean-square displacement (MSD) (Å$^2$) of (**a**) $H_2O$; (**b**) $NO_2$ and (**c**) $SO_2$ as a function of time and trend lines (straight lines) in cell(f-GSTT$_{0\%–25\%}$), respectively.

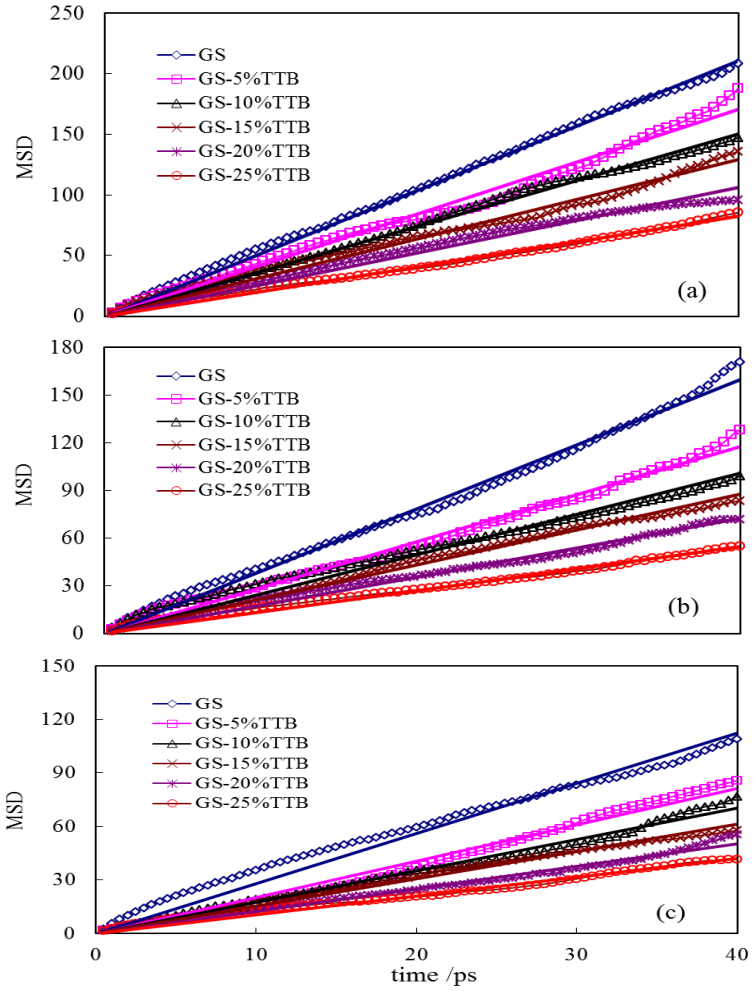


The fractional free volume between the surrounding organic chains and the inside hybrid matrix decreases in f-GSTT with the addition of TTB into the f-GS system, which is the main reason a TTB modifier enhances the anticorrosion of the GS hybrid film. The free volume is responsible for the existence of the microchannels in the hybrids, and the arranged the microchannels vary with the type of hybrids and their density. If the free volume is reduced, the penetrants ($NO_2$, $SO_2$ and $H_2O$ molecules) cannot move from one dynamic nanopore to another and permeation rates decrease [15–18]. Introduction of $TiO_2$ into the fractional free volume or having $TiO_2$ modify the free volume without occupying it, can reduce permeation in f-GSTT. With the addition of $TiO_2$ into the f-GS system, the rigid $TiO_2$ in the f-GS inhibits the intrasegmental (rotational) mobility of the chains and prevents the creation of the momentary free volume, reducing the diffusivity of $NO_2$, $SO_2$ and $H_2O$ in f-GS, blocking the formation of corrosive actions from $NO_2$, $SO_2$ and $H_2O$ composing on the AA surface and enhancing the anticorrosion of the GS hybrid film.

## 5. Conclusions

A series of new f-GSTT$_{5\%–25\%}$ coatings were able to prepare and were tested by electrochemical measurements with typical potentiodynamic polarization curves. The films coated on AA can provide

substantially superior protection efficiencies than AA and f-GS without titanium dioxide or those prepared with silica. Corrosion protection was determined from electrochemical measurements of corrosion current density, $I_{corr}$, showing in the potentiodynamic polarization curves. Analysis of the film morphology revealed that f-GSTT$_{5\%–25\%}$ had reduced micron-sized pores with increasing $TiO_2$ loadings that ultimately result in denser and less permeable coatings.

The models of cell(f-GSTT$_{0\text{-}25\%}$) can be employed to investigate SDCs by MD simulation for the $SO_2$, $NO_2$ and $H_2O$ molecules. The SDCs of $SO_2$, $NO_2$ and $H_2O$ diffusing in f-GSTT$_{5\%–25\%}$ were less than the coefficients in f-GS due to (1) the decrease in the fractional free volume between the surrounding organic chains and inside the hybrid matrix in f-GSTT$_{5\%–25\%}$ with the addition of TTB into the f-GS system; (2) the rigid $TiO_2$ in f-GSTT$_{5\%–25\%}$ which inhibited the intrasegmental (rotational) mobility of the chains and prevented the creation of the momentary free volume.

The results of the MD simulation validated the corresponding anticorrosion experiment results.

## Acknowledgments

The financial supports from the Aerospace Supporting Fund (GN: 2012-HT-HGD-11), the Invitation of Foreign Experts Program of the Chinese Foreign Experts Bureau (GN: GDW20122300078), Natural Science Foundation of HLJ Province (Key Program, GN: ZD20080201), Excellent Youth Foundation of HLJ Province (GN: JC200902) and the 9th One-Thousand Expert Plan of The Organization Ministry of the Central Government (WQ20122300100), China, are gratefully acknowledged.

## Conflicts of Interest

The authors declare no conflict of interest.

## References

1. Zhang, X.; Hu, L.; Sun, D. Nanoindentation and nanoscratch profiles of hybrid films based on (γ-methacrylpropyl)trimethoxysilane and tetraethoxysilane. *Acta Mater*. **2006**, *54*, 5469–5475.
2. Xue, Y.H.; Liu, Y.; Lu, F.; Qu, J.; Chen, H.; Dai, L.M. Functionalization of graphene oxide with polyhedral oligomeric silsesquioxane (POSS) for multifunctional applications. *J*. *Phys*. *Chem*. *Lett*. **2012**, *3*, 1607–1612.
3. Wang, H.; Lin, D.; Wang, D.; Hu, L.; Huang, Y.; Liu, L.; Loy, D.A. Computational and experimental determinations of the UV adsorption of polyvinylsilsesquioxane-silica and titanium dioxide hybrids. *Bio-Med*. *Mater*. *Eng*. **2014**, *24*, 651–657.
4. Metroke, T.L.; Kachurina, O.M.; Knobbe, E.T. Spectroscopic and corrosion resistance characterization of GLYMO TEOS ormosil coatings for aluminium alloy corrosion inhibition. *Progr*. *Org*. *Coat*. **2002**, *44*, 295–305.
5. Eisenberg, P.; Erra-Balsells, R.; Ishikawa, Y.; Lucas, J.C.; Mauri, A.N.; Nonami, H.; Riccardi, C.C.; Williams, R.J.J. Cagelike precursors of high-molar-mass silsesquioxanes formed by the hydrolytic condensation of trialkoxysilanes. *Macromolecules* **2000**, *33*, 1940–1947.

6. Wang, D.; You, H.; Hu, L. Study of three–dimensional configurations of (γ-methacryloxypropyl) silsesquioxanes by ultraviolet laser matrix–assisted desorption/ionization time-of-flight mass spectrometry and quantum chemical calculation. *Rapid Commun*. *Mass Spectrom*. **2011**, *25*, 1652–1660.
7. Liu, Y.; Sun, D.; You, H.; Chung, J.S. Corrosion resistance properties of organic-inorganic hybrid coatings on 2024 aluminum alloy. *Appl*. *Surf. Sci*. **2005**, *246*, 82–89.
8. Wang, D.; Chen, X.; Zhang, X.; Liu, Y.; Hu, L. Enhancement corrosion resistance of (γ-methacryloxypropyl) silsesquioxane hybrid films and its validation by gas-molecule diffusion coefficients using MD simulation. *J*. *Sol-Gel Sci*. *Tech*. **2009**, *49*, 293–300.
9. Behera, D.; Banthia, A.K. BisGMA/$TiO_2$ organic-inorganic hybrid nanocomposite. *Polym*. *Plast*. *Technol*. *Eng*. **2007**, *46*, 1181–1186.
10. Hu, L.; Hu, Y.; You, H. Nanoscratchprofiles of SSO Film Based on (g-methacrylpropyl)-Trimethoxysilane Modified with Titanium Tetrabutoxide. In Proceedings of the Abstracts of Papers of 245th National Spring Meeting of the American Chemical Society (ACS), New Orleans, LA, USA, 7–11 April 2013.
11. Hwang, D.K.; Moon, J.H.; Shul, Y.G.; Jung, K.T.; Kim, D.H.; Lee, D.W. Scratch resistant and transparent UV-protective coating on polycarbonate. *J*. *Sol-Gel Sci*. *Technol*. **2003**, *26*, 783–787.
12. Schmidt, H.K.; Mennig, M.; Nonninger, R.; Oliveira, P.W.; Schirra, H. Organic-inorganic hybrid materials processing and applications. *Mater*. *Res*. *Soc*. *Symp*. *Proc*. **1999**, *576*, 395–407.
13. Liu, Q.L.; Huang, Y. Structure-related diffusion in poly(methyl methacrylate)/polyhedral oligomeric silsesquioxanes. *J*. *Phys*. *Chem*. *B* **2006**, *110*, 17375–17382.
14. Karayiannis, N.C.; Mavrantzas, V.G.; Theodorou, D.N. Detailed atomistic simulation of the segmental dynamics and barrier properties of amorphous poly(ethylene terephthalate) and poly(ethylene isophthalate). *Macromolecules* **2004**, *37*, 2978–2995.
15. Meunier, M. Diffusion coefficients of small gas molecules in amorphous *cis*-1,4-polybutadiene estimated by molecular dynamics simulations. *J*. *Chem*. *Phys*. **2005**, *123*, 134906:1–134906:7.
16. Charati, S.G.; Stern, S.A. Diffusion of gases in silicone polymers: Molecular dynamics simulations. *Macromolecules* **1998**, *31*, 5529–5535.
17. Wang, D.; Zhu, P.; Wei, S.; Hu, L. Influence of molecular structure of POSS on gas-molecule diffusion coefficients using molecular dynamic simulation. *Mater*. *Sci*. *For*. **2011**, *689*, 114–121.
18. Xie, G.; Wang, P.; Hu, L. Enhancement corrosion resistance of (γ-glycidyloxypropyl)-silsesquioxane hybrid films and its validation by gas-molecule diffusion coefficients using MD simulation. *Mater*. *Sci*. *For*. **2009**, *610–613*, 190–197.
19. Kuznetsova, A.; Yates, J.T., Jr.; Zhou, G.; Yang, J.C.; Chen, X. Making a superior oxide corrosion passivation layer on Al using ozone. *Langmuir* **2001**, *17*, 2146–2152.
20. Morita, R.; Azuma, K.; Inoue, S.; Miyano, R.; Takikawa, H.; Kobayashi, A.; Fujiwara, E.; Uchida, H.; Yatsuzuka, M. Corrosion resistance of TiN coatings produced by various dry processes. *Surf*. *Coat*. *Technol*. **2001**, *136*, 207–210.
21. Jung, H.; Alfantazi, A. An electrochemical impedance spectroscopy and polarization study of nanocrystalline Co and Co–P alloy in 0.1 M $H_2SO_4$ solution. *Electrochim*. *Acta* **2006**, *51*, 1806–1814.

22. Sayed, S.Y.; El-Deab, M.S.; El-Anadouli, B.E.; Ateya, B.G. Synergistic effects of benzotriazole and copper ions on the electrochemical impedance spectroscopy and corrosion behavior of iron in sulfuric acid. *J*. *Phys*. *Chem*. *B* **2003**, *107*, 5575–5585.
23. Li, W.; Luo, J. Electric properties and pitting susceptibility of passive films formed on iron in chromate solution. *Electrochem*. *Commun*. **1999**, *1*, 349–353.
24. Spellane, P. A DC electrochemical method for studying the inhibition of metal corrosion by chromate containing paint. *Progr*. *Org*. *Coat*. **1999**, *35*, 277–282.
25. Yeh, J.; Liou, S.; Lin, C.; Yu, C.; Chang, Y.; Lee, K. Anticorrosively enhanced PMMA-clay nanocomposite materials with quaternary alkylphosphonium salt as an intercalating agent. *Chem*. *Mater*. **2002**, *14*, 154–161.